BIOCHEMISTRY
including biophysical chemistry & molecular biology

Article

pubs.acs.org/biochemistry

Investigation of Signal Transduction Routes within the Sensor/Transducer Protein BlaR1 of *Staphylococcus aureus*

Michael W. Staude, Thomas E. Frederick, Sivanandam V. Natarajan, Brian D. Wilson, Carol E. Tanner, Steven T. Ruggiero, Shahriar Mobashery, and Jeffrey W. Peng*

Department of Chemistry and Biochemistry, University of Notre Dame, Notre Dame, Indiana 46556, United States

Supporting Information

ABSTRACT: The transmembrane antibiotic sensor/signal transducer protein BlaR1 is part of a cohort of proteins that confer β-lactam antibiotic resistance in methicillin-resistant *Staphylococcus aureus* (MRSA) [Fisher, J. F., Meroueh, S. O., and Mobashery, S. (2005) *Chem. Rev. 105*, 395−424; Llarrull, L. I., Fisher, J. F., and Mobashery, S. (2009) *Antimicrob. Agents Chemother. 53*, 4051−4063; Llarrull, L. I., Toth, M., Champion, M. M., and Mobashery, S. (2011) *J. Biol. Chem. 286*, 38148−38158]. Specifically, BlaR1 regulates the inducible expression of β-lactamases that hydrolytically destroy β-lactam antibiotics. The resistance phenotype starts with β-lactam antibiotic acylation of the BlaR1 extracellular domain ($BlaR^S$). The acylation activates the cytoplasmic protease domain through an obscure signal transduction mechanism. Here, we compare protein dynamics of apo versus antibiotic-acylated $BlaR^S$ using nuclear magnetic resonance. Our analyses reveal inter-residue interactions that relay acylation-induced perturbations within the antibiotic-binding site to the transmembrane helix regions near the membrane surface. These are the first insights into the process of signal transduction by BlaR1.

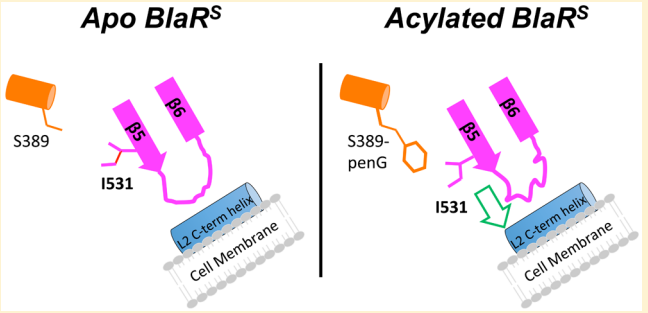

Methicillin-resistant *Staphylococcus aureus* (MRSA) is a multidrug-resistant pathogen that resists virtually all β-lactam antibiotics, the most widely used class of antibiotics in the clinic. Staphylococci use two strategies for resistance to β-lactam antibiotics. One is the expression of an altered penicillin-binding protein PBP2a, which resists inactivation by β-lactam antibiotics, as seen in MRSA strains. The other is the expression of a class A β-lactamase that hydrolytically destroys certain β-lactam antibiotics. The first system is regulated by the transmembrane β-lactam sensor/signal transducer protein MecR1 whereas the second by the cognate BlaR1, yet there are strains of staphylococci that have acquired the genes for both, *mecR*1 and *blaR*1, but have a dysfunctional *mecR*1. In these strains of MRSA, regulation of PBP2a is under the control of the protein BlaR1. Whereas BlaR1 is the better studied of the two, the two regulatory proteins are highly similar in sequence and function.[1−4] Both MecR1 and BlaR1 are transmembrane proteins that consist of four transmembrane helices, a cytoplasmic zinc protease domain, and the soluble C-terminal extracellular sensor domain ($BlaR^S$, hereafter).

The BlaR1 mechanism involves at least four steps (Figure 1, Roman numerals). (I) The β-lactam antibiotic binds and acylates a conserved serine residue within $BlaR^S$; this is the initial signal. (II) The signal is transduced through the plasma membrane to activate the cytoplasmic zinc protease domain. (III) The activated protease degrades BlaI, the repressor protein of the *bla* operon, resulting in the expression of the *bla* genes, which include the PC1 β-lactamase. Finally, in step IV, the PC1 β-lactamase is secreted outside the cell to destroy β-lactam antibiotics.

An outstanding challenge has been to identify the atomic-level changes induced by acylation that result in transmembrane signal transduction (Figure 1, steps I and II). Insights have come from previous investigations of the isolated $BlaR^S$ domain, and its interactions with β-lactam antibiotics.[1,5] For example, far-UV circular dichroism[6] and infrared[7] spectroscopies suggested some kind of conformational change in $BlaR^S$ upon acylation; however, the detailed nature of these changes remained indeterminate. Moreover, stark structural changes are unlikely, given the high degree of similarity between the X-ray crystal structures of apo $BlaR^S$ and acylated $BlaR^S$.[8,9] For example, an alignment of 231 out of 239 common Cα atoms between apo and penicillin G-acylated $BlaR^S$ showed a root-mean-square deviation (rsmd) range of 0.59−0.74 Å. Thus, while previous studies have provided valuable insights, a complete explanation remains elusive.

Another signal transduction model involves acylation-induced perturbation of the transmembrane helices (e.g., membrane helix orientation or embedding).[10] The basis for this model was phage-display studies of $BlaR^S$ in *Bacillus licheniformis*, which suggested interdomain contact between unacylated $BlaR^S$ and L2, the 56-residue extracellular loop just

Received: November 26, 2014
Revised: February 5, 2015
Published: February 6, 2015

ACS Publications © 2015 American Chemical Society

DOI: 10.1021/bi501463k
Biochemistry 2015, 54, 1600−1610

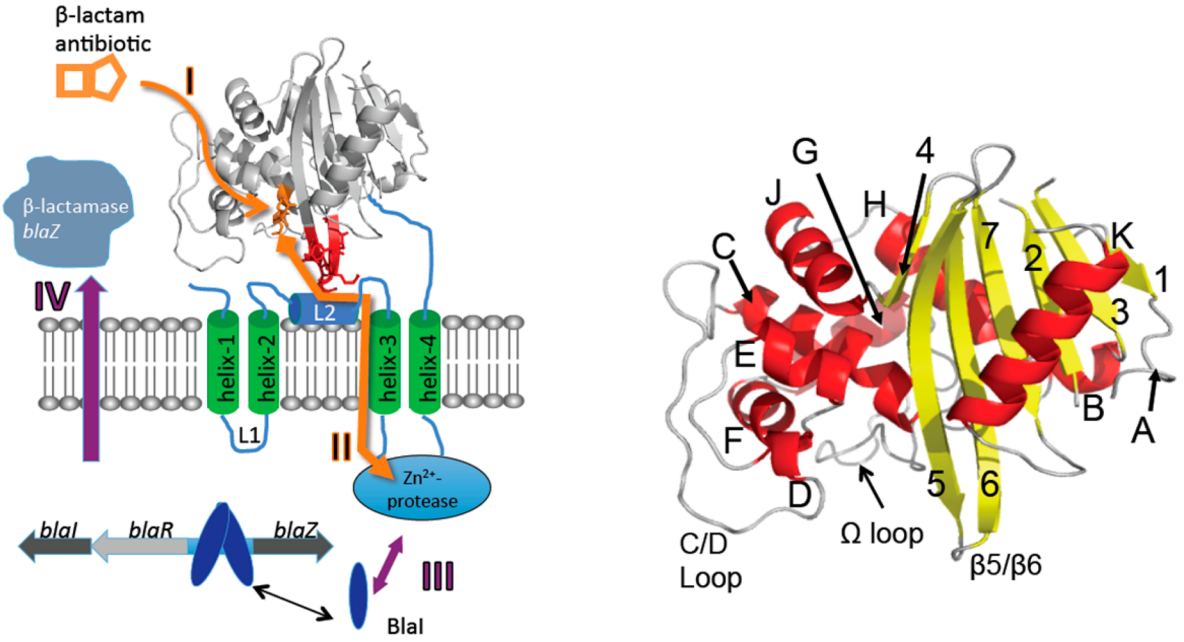

Figure 1. Overview of BlaR1 activation by β-lactam antibiotics in *S. aureus*. Important steps I–IV are detailed in the text.

preceding transmembrane helix 3 (Figure 1).[10] Acylation of $BlaR^S$ by the β-lactam antibiotic would disrupt the $BlaR^S$–L2 contact in this model. This model stipulates that disruption would perturb the directly connected transmembrane helix 3 and cytoplasmic domain, turning on the latter.

More recently, we investigated the proposed interdomain $BlaR^S$–L2 interaction at the atomic level using nuclear magnetic resonance (NMR) paramagnetic relaxation enhancement (PRE) experiments of $BlaR^S$ and a peptide corresponding to the C-terminal half of L2 ("L2short").[11] We found that L2short bound $BlaR^S$ as an amphipathic α-helix to the $\beta5/\beta6$ hairpin of $BlaR^S$, a site that is distinct from and adjacent to the $BlaR^S$ antibiotic-binding pocket. The helix bound $BlaR^S$ with its hydrophilic face, which left its hydrophobic side available for partial embedding into the plasma membrane. L2short did not block the antibiotic-binding pocket; the contact of L2short with $BlaR^S$ persisted after acylation by penicillin G (penG, henceforth), albeit, with evidence of some local rearrangement of contacts. These results raised the possibility that altered, yet sustained, contact between $BlaR^S$ and a partially membrane-embedded L2 could provide transmembrane signaling. Of course, it remains possible that acylation could disrupt the contact *in vivo*. Thus, we regard the potential consequences of acylation to the $\beta5/\beta6$–L2 interaction as forming a continuum, bounded by the extreme cases of disruption versus sustained contact.

Models invoking perturbation of the transmembrane helices are eminently reasonable, considering their intermediary location between the extracellular and cytoplasmic domains, but such models tacitly assume a coupling between acylation in the antibiotic-binding pocket and the transmembrane helix regions at the plasma membrane surface. The nature of this coupling remains obscure.

This report describes our efforts to address this knowledge gap. Specifically, we have used proton-detected ^{15}N NMR experiments to determine how acylation by penG affects $BlaR^S$. We found that acylation by penG perturbs $BlaR^S$ backbone flexibility in the antibiotic-binding pocket, and in the adjacent $\beta5/\beta6$ β-hairpin, the very same region highlighted in our previous PRE study as interacting with L2.[11] The perturbations are consistent with steric interactions between the bound antibiotic and residues in the $\beta5/\beta6$ hairpin. Together, these results and previous results indicate a contiguous path of interactions from the antibiotic-binding pocket to the membrane surface that allow transmembrane signal transduction. Acylation at Ser389 perturbs a chain of interactions from the antibiotic-binding pocket to the membrane via the interdomain contact between $\beta5/\beta6$ $BlaR^S$ and L2. The resulting perturbations to a partially embedded L2 could alter the orientation of transmembrane helices, thus affecting the portions of the protease domain associated with the cytoplasmic side of the plasma membrane.

While the subsequent events within the membrane environment remain elusive, we make a significant step forward by showing how acylation of BlaR1 by antibiotics can cause perturbations that propagate to the transmembrane helix regions at the membrane surface. These events initiate the onset of signal transduction, which are critical for unleashing of the antibiotic resistance response.

As stated above, the MecR1 protein is the cognate of BlaR1 and is found in MRSA strains. MecR1 has the same domain organization as BlaR1. Like BlaR1, the MecR1 extracellular sensor domain ($MecR^S$) transduces a signal to its cytoplasmic domain upon acylation by the antibiotic, and like BlaR1, its signal transduction is incompletely understood. Hence, insights into BlaR1 also shed light on the processes of MecR1. The two proteins are homologous on the basis of sequence analysis, microbiological response, and biochemical function.[1,4]

MATERIALS AND METHODS

Isotopically Labeled $BlaR^S$. We grew (37 °C, 240 rpm) *Escherichia coli* BL21(DE3) cells containing the pET28b plasmid encoding residues 329–585 of the *S. aureus* BlaR1 gene to an OD of ~0.7 in 1 L of LB medium. We then centrifuged and pelleted cells before resuspending them in 250 mL of M9 medium adjusted for U-^{15}N, 80% ^2D and U-$^{13}C/^{15}N$ 80% ^2D $BlaR^S$ labeling. For U-^{13}C and U-^{15}N labeling, the

DOI: 10.1021/bi501463k
Biochemistry 2015, 54, 1600–1610

medium contained [^{13}C]glucose and [^{15}N]NH_4Cl as the sole carbon and nitrogen sources, respectively. For protein deuteration, cells were grown in 100% D_2O. The cells were then incubated for 30 min (24 °C, 240 rpm) before being induced with 1 mM IPTG. After 20 h, cells were pelleted and resuspended in buffer containing 20 mM HEPES and 200 mM NaCl (pH 7.0). A total of 1.5−2 g of wet cells was lysed by sonication for a total of 6 min (10 on 50 s off) in the presence of 5 mg of hen egg white lysozyme and a Roche protease inhibitor tablet over ice. After sonication, the lysed cells were centrifuged at 35000*g* for 20 min and the supernatant was loaded onto a HI-TRAP SP cation exchange column. A salt gradient (from 200 to 800 mM NaCl) was applied after the initial protein solution flowed through, until BlaR^S eluted. Fractions were pooled and loaded onto an S200 gel-filtration column pre-equilibrated with 20 mM NaH_2PO_4 and 150 mM NaCl to separate contaminating proteins and yield a purified sample. Fractions were collected and exchanged into the final NMR buffer (20 mM NaH_2PO_4 and 30 mM NaCl in a 90/10 H_2O/D_2O mixture and 0.02% NaN_3.) All NMR samples were at a BlaR^S concentration of 300 μM. The nominal NMR probe temperature was set to 282 K to achieve a sample temperature of 278 K, as determined by measurement of a methanol temperature standard.

Sequential NMR Assignments of Apo and Acylated BlaR^S. For sequential assignments of the backbone, we used standard TROSY-based three-dimensional (3D) NMR experiments (HNCA, HNCOCA; HNCO, HNCACO; HNCACB, HNCOCACB) on U-^{15}N,^{13}C, 80% ^{2}D BlaR^S.[12] Time domain data were processed using Topspin 2.1 (Bruker Biospin, Inc.). Sequential backbone assignments were made using SPARKY[13] and CARA.[14] To acylate BlaR^S, we titrated in penG (Sigma-Aldrich) and monitored the resulting perturbations to the NH chemical shift perturbations via two-dimensional (2D) ^{15}N−^{1}H TROSY-HSQC.[15] The NH chemical shift perturbations (CSPs, $\Delta\delta$) were calculated as

$$\Delta\delta = \sqrt{{\delta_{1H}}^2 + (0.154\delta_N)^2} \tag{1}$$

The CSPs essentially ceased after achieving a 1:1 ratio; however, we continued additions to a final 10:1 molar excess of penG over BlaR^S to ensure detection of the acylated state throughout the NMR experiments. The CSPs were sufficiently extensive (Figure S1, Supporting Information) that we performed additional 3D NMR experiments to reassign penG-acylated BlaR^S (penG-BlaR^S).

Backbone ^{15}N Relaxation Experiments. To characterize the backbone flexibility of apo and acylated BlaR^S, we measured standard backbone NH relaxation rate constants, including ^{15}N R_1, R_2, and ^{15}N−^{1}H steady-state NOE. The relaxation experiments were conducted at 16.4 T (700 MHz ^{1}H frequency) and 278 K. The R_1 series consisted of nine experiments with relaxation delays (s) of 0.048 (twice), 0.192, 0.400, 0.592, 0.800, 1.040, 1.344, and 1.552. The R_2 series consisted of nine experiments with relaxation delays of 8.24 (twice), 16.48, 24.72, 32.96, 41.20, 49.44, 57.68, and 65.92 ms. The steady-state NOE experiments were recorded as interleaved 2D spectra alternating between saturating and nonsaturating conditions. Saturation was achieved via 5 s of proton saturation, using the pulse scheme of Ferrage et al.[16] All relaxation series time domain data were processed in Topspin 2.1 (Bruker Biospin, Inc.). The cross-peaks were integrated and fit to single-exponential decay functions using in-house software. Errors were calculated from Monte Carlo simulations of the data based on integral uncertainties estimated from the duplicate time points.

Reduced Spectral Density Mapping. To convert the relaxation rates into dynamics information, we used the reduced spectral density mapping procedure,[17−19] which has the advantage of yielding site-specific dynamics parameters directly from the measured rate constants via simple linear relationships. The specific conversion formulas used were those specified by Peng and Wagner[19]

$$J_{eff}(0) = \frac{3}{2(3D + C)}\left(R_2 - \frac{R_1}{2} - \frac{3\sigma_{NH}}{5}\right)$$
$$J(\omega_N) = \frac{1}{3D + C}\left(R_1 - \frac{7\sigma_{NH}}{5}\right)$$
$$\langle J(\omega_H)\rangle = \frac{\sigma_{NH}}{5D} \tag{2}$$

As shown previously, $J_{eff}(0)$ is the most sensitive probe of local flexibility,[19] and we used it as our primary site-specific dynamical parameter. It has two contributions, $J(0)$ and λR_{ex}:

$$J_{eff}(0) = J(0) + \lambda R_{ex} \tag{3}$$

$J(0)$ describes the faster dynamics: picosecond (10^{-12} s) to nanosecond (10^{-9} s) reorientational motions of the NH bond relative to the static magnetic field. In the well-known Lipari−Szabo formalism,[20,21] $J(0)$ is dominated by the product $\mathbf{S}^2\tau_m$, where τ_m is the correlation time for overall solution tumbling and $\mathbf{S}^2$ is the amplitude of internal motion. The second term, λR_{ex}, reflects the slower dynamics: microsecond (10^{-6} s) to millisecond (10^{-3} s) exchange dynamics that modulate the ^{15}N chemical shift that can broaden the ^{15}N line width.

NH Hydrogen Exchange. To explore the possibility of structural changes in BlaR^S upon penG acylation, we performed NH hydrogen exchange (HX) experiments using the WEX-III TROSY methods.[22] Measurements consisted of a series of spectra acquired at four pH values (6.06, 6.91, 7.60, and 8.13) at 16.4 T and 278 K for apo and penG BlaR^S, respectively. Each series consisted of a reference experiment to allow for complete R_1 ^{1}H relaxation to occur, and two experiments in which the water resonance was inverted using a 2 ms isnob3 pulse,[23] or maintained along +*Z*, prior to mixing times of 20, 50, 75, 100 (twice), 150, 300, and 400 ms. The spectra were then processed using Topspin 2.1. Using in-house software, we integrated the amide cross-peaks to give intensity versus T profiles, $S(T)$, which we then fit to eq 4 below:[22]

$$S(T) = \frac{M_Z^+(T) - M_Z^-(T)}{2M^0} = \frac{\Delta f k_{obs} e^{-R_{1W}T}}{R_1' + k_{obs} - R_{1w}}[1 - e^{-(R_1' + k_{obs} - R_{1W})T}] \tag{4}$$

The adjustable parameters of eq 4 included the following: $k_{obs} = k_{H_2O} + k_{NOE}$ and $R'_1 = R_1 - k_{NOE}$. R_{1W} (longitudinal relaxation rate constant of water) and Δf (fractional steady-state water signal) values were predetermined for each series, following the procedure of Fitzkee et al.[22] Errors were calculated from Monte Carlo simulations based on intensity differences between duplicate time points. The observed increase in k_{obs} versus pH suggested an EX2 mechanism;[24] therefore, k_{H_2O} and k_{NOE}, and thus the R_1 contribution to R'_1,

DOI: 10.1021/bi501463k
Biochemistry 2015, 54, 1600−1610

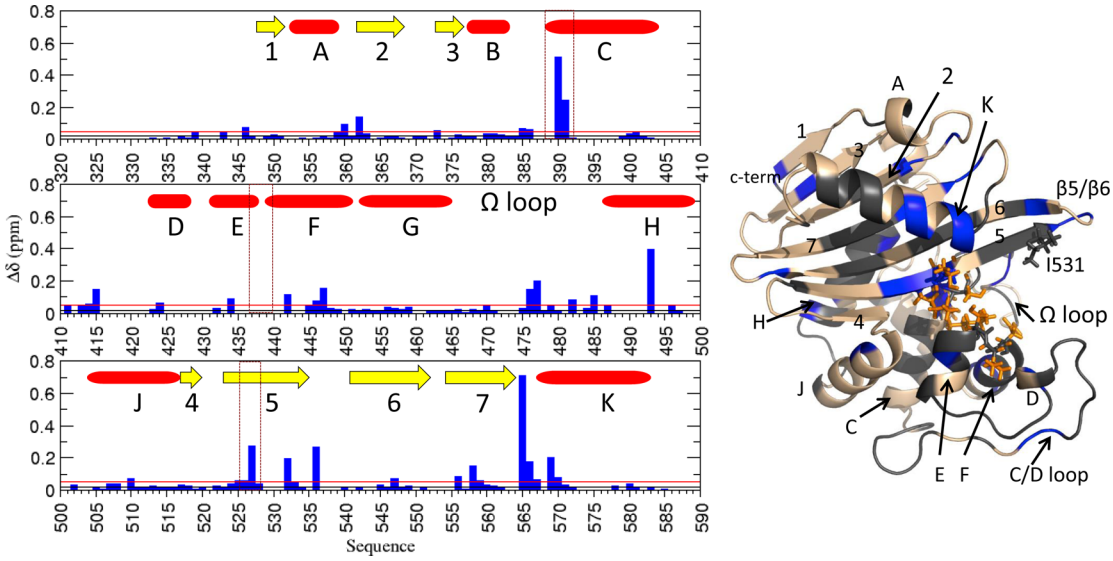

Figure 2. NH chemical shift perturbations of BlaR^S induced by penG. Blue shading on the structure denotes residues with CSP magnitudes of >0.050 (two standard deviations). Wheat shading denotes amides with CSP magnitudes of <0.050. Dark gray shading denotes residues lacking assignments in one or both states. Orange sticks highlight active-site residues nearest the bound penG. In the bar chart, yellow arrows and red cylinders refer to β-strands (numbers) and α-helices (letters), respectively. The rectangular boxes highlight conserved residue motifs among bacterial acyltransferases,[27] S-xx-K (S389, T390, Y391, and K392), S/T-x-N, (S437, V438, and N439), and KT/SG (K526, T527, and G528).

were calculated by fitting the pH dependence of k_{obs} to eq 5, using a reference pH^0 of 7.0. Statistical uncertainties were estimated using the rmsd of the first fit. For residues lacking significant pH dependence of k_{obs}, the k_{NOE} value was the average of the k_{obs} value at all pH values. The slowest detected k_{H_2O} was 0.020 s^{-1}, while the fastest was 30 s^{-1}.

$$k_{obs}(pH) = k_{NOE} + k_{H_2O} \times 10^{(pH-pH^0)} \quad (5)$$

Light Transmission Spectroscopy (LTS). LTS uses wavelength-dependent light extinction that allows the characterization of nanoparticles including proteins by size, shape, and density.[25,26] LTS measures the transmission (at zero angle with respect to the incoming beam) of light through the protein sample as a function of wavelength, and the extinction is inverted to obtain the protein size distribution. The dynamic range that LTS can be applicable is in the low-volume fraction regime (5×10^{-8} to 0.5 vol %). LTS measurements for apo and penG-acylated BlaR^S were taken at 278 K. Samples consisted of 1 mL of ~30−60 μM (~2−4 $\times$ 10^{16} particles) BlaR^S (with or without penG) and blanks of phosphate buffer blank (with or without penG). Prior to the measurements, all samples were filtered with 20 nm sterile filters (Anotop 10, Whatman Filters) to minimize the interference of particle size within the range of 300−3000 nm.

RESULTS

Our BlaR^S construct has 256 residues, five of which are prolines, leaving 251 backbone amide NH bond vectors. We could assign only ~66% of the backbone for both the apo state of BlaR^S (apo-BlaR^S) and the penG-acylated state (penG-BlaR^S). Missing resonances, stemming from exchange broadening or resonance overlap, precluded complete backbone assignment.

The missing sequential assignments in apo and acylated BlaR^S differed somewhat, because of the chemical shift changes, which in turn altered the pattern of resonance overlap and exchange broadening (Figure S2, Supporting Information). Varying the sample temperature for either apo or acylated BlaR^S between 278 and 298 K did not sufficiently enhance the spectral quality for complete assignments. The assignments, while incomplete, were sufficient to give insights into the consequences of acylation, as described below.

Acylation of BlaR^S Causes Widespread Chemical Shift Perturbations in BlaR^S. Adding a 10-fold molar excess of penG to BlaR^S produced persistent and significant backbone NH chemical shift perturbations (CSPs) (Figure 2). The average over the CSPs was 0.020 ± 0.015 ppm. Prominent CSPs occurred at residue groups defining the BlaR^S antibiotic-binding pocket and included (i) helix C residues, S389 (the acylated serine), T390, Y391, and K392; (ii) helix F residues, such as F442, I445, S446, and D447; (iii) Ω loop residues, such as L468, K472, W475, M476, E477, and D478; (iv) β5 residues, such as K526, T527, and G528; and (v) β5/β6 hairpin residues V532, N533, and Y536. These CSPs coincided with or were adjacent to the three motifs conserved among numerous bacterial acyltransferases.[1,5,27] In particular, groups (i), (ii), and (iv) corresponded to the "S/T-xx-N" (x is any amino acid), "S/T-x-N", and "KTS/G" motifs, respectively. We also noted that group (v) was the very same β5/β6 hairpin that emerged in our previous PRE study as the binding site for extracellular loop L2.[11] These residues are close to the covalently bound penG in the X-ray crystal structure of Protein Data Bank (PDB) entry 1XA7.[8]

Significant CSPs also occurred for several residue groups outside the antibiotic-binding pocket. One group included residues bracketing or residing within the disordered loop between α-helices C and D, such as D401, R411, S413, and D422 (Figure 2, bottom of the structure). Another group consisted of residues of α-helix H, just after the Ω loop, and included I482, L485, and Q487 (not visible in the protein orientation presented here). Finally, a third group included residues of the C-terminal α-helix K (S564—M579), including S564, G565, K566, A568, E569, and L570. We consider the origins of these more remote CSP sites in the Discussion.

DOI: 10.1021/bi501463k
Biochemistry 2015, 54, 1600−1610

Intrinsic Flexibility of Apo BlaR^S. We investigated the flexibility of the backbone NH bonds in apo-BlaR^S at 16.4 T and 278 K using 2D TROSY ^{15}N spin relaxation experiments (R_1, R_2, and heteronuclear dipolar cross-relaxation rate σ_{NH}). We used more recent pulse schemes, modified to reduce artifacts caused by rapid NH solvent exchange.[16,28,29]

After excluding resonances suffering overlap or a poor signal-to-noise ratio, we had data for 128 NHs for apo-BlaR^S. The trimmed averages and standard deviations for the ^{15}N relaxation parameters were as follows: $\langle R_{1,apo}\rangle$ = 0.42 ± 0.02 s^{-1}, $\langle R_{2,apo}\rangle$ = 41.0 ± 1.5 s^{-1}, and $\langle ssNOE_{apo}\rangle$ = −0.200 ± 0.05. We extracted dynamic parameters from the relaxation rates using reduced spectral density mapping.[17−19] The principal moments of inertia for apo BlaR^S (PDB entry 1XKZ) are 1.0, 1.0, and 0.7, indicating only slight overall shape anisotropy. Hence, we interpreted site-specific variation in $J_{eff}(0)$ as being reflective of variations in local NH mobility, per eqs 2 and 3. Accordingly, high and low outliers of $J_{eff}(0)$ indicated microsecond to millisecond exchange dynamics and subnanosecond internal motions, respectively.

The trimmed average and standard deviation of $J_{eff}(0)$ was 11.0 ± 0.5 ns/rad. The largest and smallest $J_{eff}(0)$ values were in the Ω loop [S470, $J_{eff}(0)$ = 15.4 ns/rad] and N-terminus [S333, $J_{eff}(0)$ = 1.8 ns/rad], respectively. Figure 3 maps the apo-state $J_{eff}(0)$ onto the apo BlaR^S X-ray crystal structure (PDB entry 1XA7).[8] The deep salmon and marine shadings denote high and low deviations relative to the aforementioned trimmed average (11.0 ± 0.5 ns/rad), respectively. In the context of eq 3, the deep salmon shading pinpoints NH bonds with exchange dynamics on the microsecond to millisecond time scale, while marine shading pinpoints bonds with enhanced reorientational motions on the subnanosecond time scale.

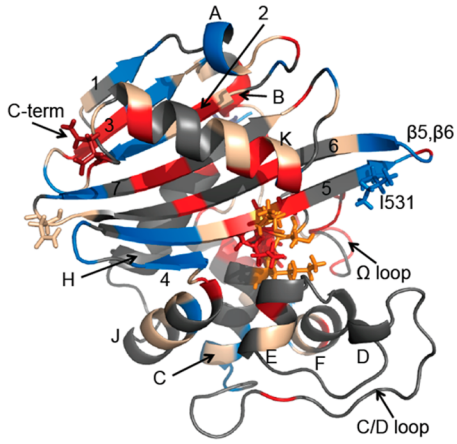

Figure 3. Intrinsic backbone flexibility of apo BlaR^S, via $J_{eff}(0)$. Red shading indicates regions where $J_{eff}(0)$ is higher than average (enhanced exchange dynamics). Marine shading indicates regions where $J_{eff}(0)$ is lower than the average (enhanced subnanosecond bond mobility). Wheat shading indicates regions included in the core average. Dark gray shading indicates regions lacking data in the apo form.

Sites of exchange dynamics, the high outliers (deep salmon), were predominant in the core. This included the antibiotic-binding pocket and more remote β-strands and parts of α-helix K. Sites of enhanced subnanosecond mobility, the low outliers (marine), were toward the protein exterior, mainly at the β-hairpins. Of note, the β5/β6 hairpin gave clear evidence of intrinsic conformational flexibility, involving both subnanosecond reorientational dynamics and microsecond to millisecond exchange dynamics. Bar charts and numerical values for apo $J_{eff}(0)$ are given in Figure S3 and Table S1 of the Supporting Information.

Acylation by penG Alters NH Backbone Flexibility. We repeated the backbone dynamics analysis for penG-BlaR^S using the same experiments, temperature, and field strength. For penG-BlaR^S, 130 NHs could be analyzed, as compared to 128 for apo-BlaR^S. From these, we identified a common set of 104 NH sites for relaxation analysis (~42% of non-proline residues). The trimmed averages and rmsds for the ^{15}N relaxation parameters were as follows: $\langle R_{1,penG}\rangle$ = 0.43 ± 0.02 s^{-1}, $\langle R_{2,penG}\rangle$ = 38.5 ± 1.5 s^{-1}, and $\langle ssNOE_{penG}\rangle$ = −0.210 ± 0.06.

A reduced spectral density mapping analysis of the penG-BlaR^S relaxation rates gave an average and rmsd for $J_{eff}(0)$ of 10.2 ± 0.2 ns/rad. This average value was slightly lower than the average value for apo-BlaR^S (11.0 ± 0.5 ns/rad). The difference was due to a slight increase of ^{15}N R_2 values for apo BlaR^S versus penG-BlaR^S, for nearly all residues (i.e., $\langle R_{2,apo}\rangle$ = 41.0 ± 1.5 s^{-1} vs $\langle R_{2,penG}\rangle$ = 38.5 ± 1.5 s^{-1}). The global increase suggested apo-BlaR^S might undergo a global exchange process, such as nonspecific aggregation, or transient dimerization, that contributes a small and global R_{ex} to $J_{eff}(0)$, per eq 2.

Accordingly, we investigated the possibility of dimerization using light transmission scattering (LTS)[25,26] on BlaR^S samples at concentrations as low as 30 μM. The LTS results indicated two populations for apo BlaR^S, with effective radii differing by a factor of 2 (Figure S4, Supporting Information). Population analysis was not available from this approach. We corroborated the LTS results with matrix-assisted laser desorption ionization mass spectrometry of apo BlaR^S, which revealed a species at 60 kDa, essentially twice the molecular mass of the monomer BlaR^S (30 kDa). The 60 kDa peak was at a very low intensity compared to that of the 30 kDa peak, suggesting a small relative population (Figure S5, Supporting Information). Thus, both LTS and mass spectrometry suggested some residual dimerization. On the other hand, previous X-ray crystallography and static light scattering studies of BlaR^S gave no indication of dimerization.[8] Moreover, our numerous ^{15}N−^{1}H spectra of apo or acylated BlaR^S lacked an obvious set of secondary NH cross-peaks. Combining the results mentioned above, we suspect apo BlaR^S undergoes rapid chemical exchange between a major monomer population and a minor dimer population, whose NMR signals must be very weak and close to the noise floor. Acylation by penG pushes the equilibrium toward the monomer species, leading to a global decrease in the measured ^{15}N R_2 and $J_{eff}(0)$ from apo BlaR^S to acylated BlaR^S. In passing, we note that BlaR1 has a very low copy number in the *S. aureus* membrane.[3] This suggests that the minor dimerization inferred in our *in vitro* studies is not likely a functional feature of the BlaR1 mechanism.

To compare the conformational flexibility of apo and acylated-BlaR^S, we needed to account for the global offset in $J_{eff}(0)$. Hence, we used the dimensionless site-specific ratio

$$\frac{\Delta J}{J_{eff}^{apo}(0)} = \frac{J_{eff}^{apo}(0) - J_{eff}^{penG}(0)}{J_{eff}^{apo}(0)} \quad (6)$$

We then subtracted off the trimmed average of this ratio (0.063) to identify those NH sites with values beyond one

DOI: 10.1021/bi501463k
Biochemistry 2015, 54, 1600−1610

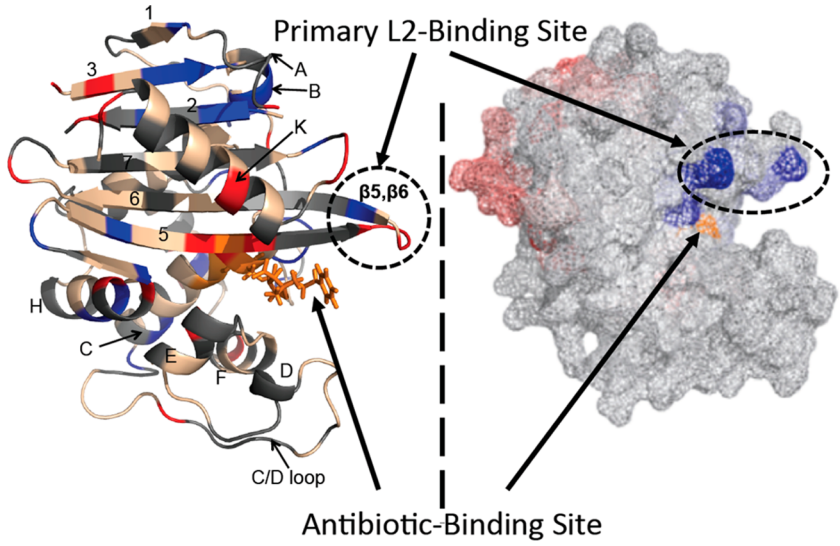

Figure 4. Changes in NH $J_{eff}(0)$ caused by penG acylation. The left panel shows a map of the fractional change, $\Delta J/J_{eff}^{apo}(0) = 1 - J_{eff}^{penG}(0)/J_{eff}^{apo}(0)$. Colored sites are sites for which the magnitude of fractional changes was >0.025 from the core average. Red shading indicates positive values [acylation decreases $J_{eff}(0)$], and blue shading indicates negative values [acylation increases $J_{eff}(0)$]. Wheat shading denotes residues with fractional changes consistent with the core average ± two standard deviations, while dark gray shading indicates residues lacking data in one or both states. The right panel shows the paramagnetic relaxation enhancement (PRE) response of amide protons in ^{15}N-labeled BlaR^S, upon interaction with the spin-labeled L2short peptide.[11] Blue denotes the strongest interaction site and red a weaker nonspecific interaction.

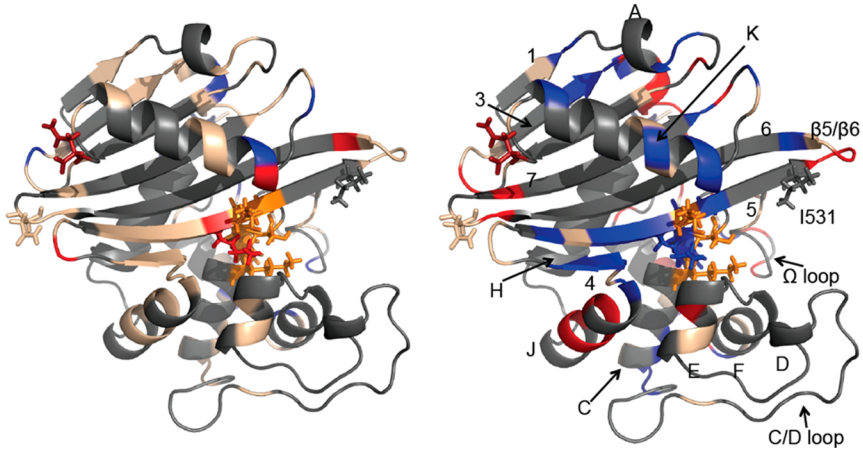

Figure 5. Amide hydrogen exchange response of BlaR^S upon penG acylation. The left panel shows a map of $\Delta k_{H_2O}/k_{H_2O}^{apo}$. Colored shading denotes sites for which the magnitude of the fractional changes is more than one standard deviation from the core average. Blue shading indicates residues for which acylation decreases k_{H_2O} (negative $\Delta k_{H_2O}/k_{H_2O}^{apo}$), and red shading indicates residues for which acylation increases k_{H_2O} (positive $\Delta k_{H_2O}/k_{H_2O}^{apo}$). Wheat shading indicates residues lacking significant differences in k_{H_2O}. Dark gray shading indicates residues lacking data in one or both states. In the right panel, blue highlights k_{NOE} fractional changes more than one standard deviation from the core average (decreased level of exchange upon acylation). Red highlights residues with k_{NOE} fractional changes less than one standard deviation from the core average (increased level of exchange upon acylation). Wheat shading indicates residues lacking significant differences in k_{NOE}. Dark gray shading indicates residues lacking data in one or both states.

standard deviation (0.025) from the trimmed average. The results are shown in Figure 4 (left panel), with red and blue shading indicating the changes per eq 6. Bar charts and numerical values of $J_{eff}(0)$ for penG-acylated BlaR^S are given in Figure S6 and Table S2 of the Supporting Information.

In Figure 4, red shading indicates $J_{eff,apo}(0) > J_{eff,penG}(0)$, a decrease upon penG acylation, while blue shading indicates the opposite. The antibiotic-binding pocket and the bound PenG (orange sticks) showed significant dynamical changes, which consisted mainly of decreases in $J_{eff}(0)$ upon acylation (red shading). Per eq 2, these decreases in $J_{eff}(0)$ could indicate that acylation caused an increase in the amplitudes of subnanosecond bond motion (reorientational bond motions), the reduction of apo-state R_{ex}, or both. To identify the most likely scenario, we note that many of these NH sites showed evidence of R_{ex} in apo-BlaR^S [i.e., larger $J_{eff}(0)$, deep salmon shading in Figure 3]. Hence, the reduction upon penG acylation most likely reflects the reduction of R_{ex} contributions in the apo-state chemical exchange dynamics inherent to the vacant binding pocket.

Other sites of dynamic change involved an increase in $J_{eff}(0)$ upon penG acylation (blue shading). This could indicate that acylation decreased the amplitudes of subnanosecond bond motion, stimulated new chemical exchange processes (R_{ex}), or

DOI: 10.1021/bi501463k
Biochemistry 2015, 54, 1600−1610

both. To identify the most probable scenario, we note that most of the blue-shaded sites in Figure 4 (left panel) lacked evidence of chemical exchange processes in apo BlaR^S (Figure 3). Thus, their increase in $J_{eff}(0)$ upon penG binding most likely indicates an acylation-induced increase in $J(0)$, per eq 2: they are NH bonds that become more rigid on the subnanosecond time scale.

Significantly, the $\beta5/\beta6$ hairpin (I531−K535) showed signs of dynamic change on both slow and fast time scales. Thus, acylation by penG perturbs the conformational flexibility of residues that interact with extracellular loop L2.[11]

NH Hydrogen Exchange. To investigate collective structural fluctuations on longer time scales (milliseconds to seconds), we measured hydrogen exchange (HX) rate constants for the backbone amide protons of apo and penG-acylated BlaR^S, using the WEX-III ^{15}N−^{1}H TROSY pulse scheme.[22] This pulse scheme permits millisecond time resolution and provides enhanced sensitivity for larger proteins. The HX measurements were taken at the same temperature and static field strength used for the ^{15}N spin relaxation rates mentioned above (278 K and 16.4 T, respectively). Furthermore, they were conducted at four pH values (6.06, 6.91, 7.60, and 8.13).

The HX rate constants (k_{H_2O}) were consistent with expectations based on the BlaR^S crystal structures (PDB entry 1XA7),[8] in that regions of well-defined secondary structure displayed no detectable hydrogen exchange within our time window (20−400 ms), while solvent-exposed loops and turns displayed the highest k_{H_2O} rate constants. Figure S7 (left panels) of the Supporting Information shows the general distribution of k_{H_2O} values, with red shading indicating enhanced hydrogen exchange (larger k_{H_2O}). Numerical values are listed in Table S1 of the Supporting Information. The k_{H_2O} values ranged from 0.02 to 30 s^{-1}, with uncertainties averaging 40−50% of the measured value. WEX-III TROSY also provided site-specific k_{NOE} rate constants, which report on the local density of hydroxyl protons in rapid exchange with bulk water. The distribution of k_{NOE} values of apo-BlaR^S was also consistent with the crystal structure in that amide protons with spatially proximal hydroxyl side chains (Ser, Thr, and Tyr) showed k_{NOE} values much higher than the values of those without. This is apparent in Figure S7 (right panel) of the Supporting Information; the corresponding values are listed in Table S1 of the Supporting Information.

To determine the effects of penG acylation on the HX rate constants, we added a 10-fold molar excess of penG to BlaR^S and repeated the WEX-III TROSY measurements. Figure 5 shows the resulting fractional changes. The resulting penG-BlaR^S k_{H_2O} profile was very similar to that of apo-BlaR^S and thus corroborated the notion that acylation preserves the overall structure. Most k_{H_2O} rate constants showed no significant differences (Figure 5, left, red and blue shading indicating increased and decreased k_{H_2O} values, respectively). The handful of significant k_{H_2O} changes occurred at sites distal from the active site, with the exception of the start of α-helix K.

Changes upon acylation were more evident in k_{NOE} (Figure 5, right panel). The average and rmsd fractional change was 17 ± 4%. Acylation yielded significant decreases in k_{NOE} within the antibiotic-binding pocket, and the surrounding regions (in particular, α-helix K). Numerical values for k_{H_2O} and k_{NOE} for acylated BlaR^S are listed in Table S2 of the Supporting Information.

DISCUSSION

The mechanism that couples acylation of BlaR^S to the transmembrane regions remains obscure. A reasonable hypothesis is that it involves a perturbation of transmembrane helices (e.g., TM-3 and/or TM-4).[10] For this hypothesis to be tenable, there should be intramolecular interactions to couple acylation within the antibiotic-binding pocket to the transmembrane helix regions at the membrane surface. Hitherto, those interactions have not been forthcoming.

Accordingly, we have used NMR to investigate how acylation affects the BlaR^S conformational ensemble in solution. NMR provides a comprehensive and site-specific description of both protein conformation and flexibility and is an excellent complement to previous X-ray crystallography[8,9] and optical spectroscopy[6,7] studies of BlaR^S. We measured and compared backbone chemical shifts, spin relaxation parameters, and amide hydrogen exchange rates for apo and penG-acylated BlaR^S at 278 K. We discuss these changes below and their significance to BlaR^S transmembrane signal transduction.

Acylation-Induced Chemical Shift Perturbations of NH Bonds. As indicated in Figure 2, many of the residues showing acylation-induced chemical shift perturbations (CSPs) are in or near the antibiotic-binding pocket and are therefore close to the covalently bound penG (PDB entry 1XA7[8]). These CSPs likely reflect the spatial proximity to the penG phenyl side group (ring current effects) or local shifts in hydrogen bonding caused by penG acylation. Many of these CSP-bearing residues are conserved among structural homologues of BlaR^S, as discussed by Wilke et al.[8] (i.e., the BlaR1 sensor domains from *B. licheniformis* and *Staphylococcus hemolyticus*, MecR1 sensor domains from *S. aureus* and *Staphylococcus epidermidis*, and the class D β-lactamase OXA-10 from *Pseudomonas aeruginosa*[8]). These same CSPs encompass residue motifs conserved among numerous bacterial acyltransferases,[27] such as the S-xx-K motif (S389, T390, Y391, and K392 in helix C), and the KTS/G motif (K526, T527, and G528 in β5). We could not ascertain CSPs for the third S/T-x-N motif because of the missing resonances (S437, V438, and N439 between α-helices E and F).

The origins of the CSPs outside the active site are less clear. They coincide with, or are close to, residues that are conserved across BlaR^S homologues, but lacking direct contact with penG.[8] Examples are CSP-bearing residues of the flexible loop (residues D401—P420) between α-helices C and D, including D401, R411, S413, and D422, which bracket the strictly conserved W414. Other examples are CSPs at I482, L485, and Q487; these residues bridge the Ω loop with α-helix H and coincide with, or are next to, the conserved residues S483, Q487, and V488.

Particularly intriguing were the CSP-bearing residues in α-helix K (S564, G565, K566, A568, E569, and L570). This helix neighbors the antibiotic-binding pocket but is spatially distinct. Moreover, it harbors only one conserved residue, I575. Why this region should be perturbed by acylation is not obvious. One possibility, discussed further below, involves the formation of new binding pockets similar to those observed in a recent computational study of another BlaR^S homologue, the class A β-lactamase, TEM-1 (PDB entry 1JWP).[30]

Weak Dimerization. The apo BlaR^S ^{15}N relaxation data showed a slight, global (i.e., all NH sites) increase in R_2 over

DOI: 10.1021/bi501463k
Biochemistry 2015, 54, 1600−1610

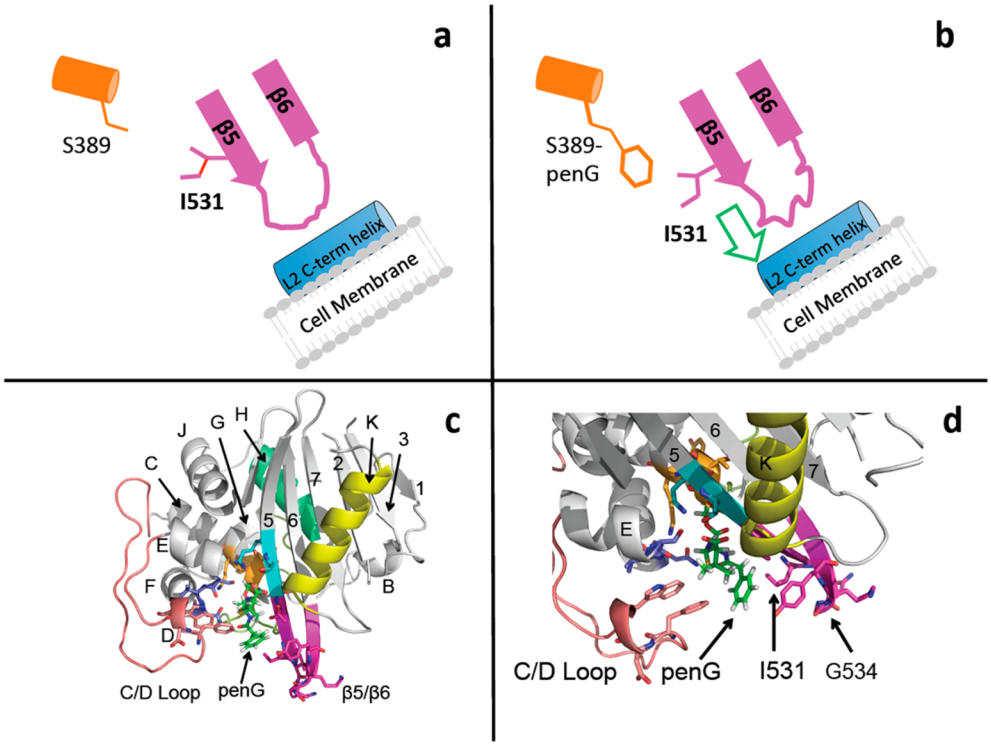

Figure 6. Proposed mechanism for BlaR1 signal transduction. Transduction involves a contiguous chain of interactions that include the side chain substituent of the covalently bound antibiotic, the $\beta5/\beta6$ hairpin, and extracellular loop L2. Our previous results[11] indicated that L2 binds $\beta5/\beta6$ as an amphipathic helix that could partially embed into the membrane. (a) In the apo state, $\beta5/\beta6$ interacts with the L2 helix. (b) Acylation of Ser389 by a β-lactam antibiotic results in new interactions between the antibiotic side chain and bulky protein side chains of $\beta5/\beta6$, such as Ile531, which then perturb the $\beta5/\beta6$–L2 interaction. The effects propagate from L2 to its connecting transmembrane helix and onto the cytoplasmic Zn^{2+} protease domain, stimulating β-lactamase production. (c and d) Full view and close-up, respectively, of the interaction chain based on PDB entry 1XA7. Green sticks highlight the bound antibiotic penG (the phenyl moiety of its C6 substituent). Magenta shading and sticks highlight the $\beta5/\beta6$ region and its residues (I531 and G534). Deep salmon shading denotes the disordered C/D loop that shows local dynamic changes upon acylation. Yellow shading denotes α-helix K, implicated in cryptic allostery.[30] Orange, slate, and aquamarine shading show S-xx-K, S/T-x-N, and KT/SG motifs, respectively, conserved among bacterial acyltransferases.[27] The proposed interaction between the antibiotic C6 substituent and I531 is supported by the work of Mobashery and co-workers,[37] which showed that β-lactam antibiotics with larger substituents are better inducers, and the fact that related proteins that are enzymes (e.g., OXA-10) instead of transducers lack the bulky hydrophobic side chain at this position.

that of the penG-acylated state ($\langle R_{2,apo}\rangle$ = 41.0 ± 1.5 s^{-1} vs $\langle R_{2,penG}\rangle$ = 38.5 ± 1.5 s^{-1}). This observation, along with LTS and mass spectrometry measurements, suggests that apo $BlaR^S$ exchanges rapidly between a dominant monomer species and a minor dimer species under our NMR experimental conditions. We looked for experimental indicators of a possible dimerization surface,[11] yet additional NH cross-peaks were not obvious; the only indicator of a possible dimer interface was from our previous PRE studies, which showed nonspecific binding of L2 to the $\beta6/\beta7$ hairpin. However, this interaction was quite weak (K_d > 1 mM) and easily disrupted by an increasing ionic strength.[11] If this putative monomer–dimer exchange is fast on the relaxation time scale ($k_{ex} \gg |R_{2,dimer} - R_{2,monomer}|$) and $BlaR^S$ tumbles according to the simple Stokes–Einstein relationship adjusted for temperature effects,[31] then the global increase in R_2 suggests a minor dimer population of 4–6%.

Previous X-ray crystallography studies of apo versus penG-acylated $BlaR^S$[8] gave no evidence of apo-state dimerization, and penG was seen only in the context of a monomer form. Moreover, the low copy number of BlaR1 in *S. aureus*[3] argues against dimerization playing a functional role for the protein. Combining these facts with those of the preceding paragraph suggests the weak apo-state dimerization is a residual and nonspecific effect.

Acylation-Induced Changes in Backbone Flexibility. After adjusting for the small R_2 offset between the apo and penG states (see above), we could assess the response of $BlaR^S$ backbone flexibility to acylation. The response of the entire backbone to acylation cannot yet be determined, because of missing resonance assignments. Nevertheless, it is clear that $BlaR^S$ has intrinsic conformational flexibility at its functional sites, which changes in response to acylation by penG.

For example, the enhanced $J_{eff}(0)$ values (Figure 3, deep salmon shading) decorate the protein interior and include the buried regions of central β-strands 5–7 and the active site. These enhancements indicate exchange broadening caused by microsecond to millisecond exchange dynamics in the protein "gut", suggesting a conformational flexibility conducive to antibiotic entry. Acylation partially attenuates the exchange broadening (smaller R_{ex} term, per eq 2). The attenuation could reflect changes in the fractional populations of the underlying exchange-coupled states, changes in chemical shifts, or changes in the rate constants for interstate hopping.

On the other hand, residues toward the protein surface, particularly those toward the β-hairpins, show reduced $J_{eff}(0)$ values in apo $BlaR^S$, suggesting enhanced reorientational flexibility of the NH bond vector on the subnanosecond time scale. Acylation increases their $J_{eff}(0)$, suggesting an increase in local rigidity.

DOI: 10.1021/bi501463k
Biochemistry 2015, 54, 1600–1610

Most notably, acylation changed the local dynamics of the β5/β6 hairpin (I531−K535) on both slow and fast time scales. Thus, acylation perturbs the conformational flexibility of residues that interact with extracellular loop L2.[11] These residues are right next to K526, T527, and G528, which showed strong CSPs and are fully conserved across the aforementioned BlaR^S homologues. Additionally, the side chain of I531 is close to the phenyl moiety of the C6 substituent of penG; hence, the internal mobility of this residue is sensitive to penG. These observations suggest the functional importance of the β5/β6 motion, and they are central to our model for signal transduction, as described below.

NH Hydrogen Exchange. Previously, Joris and co-workers used infrared spectroscopy to investigate hydrogen exchange in *B. lichenformis* BlaR^S[10] (temperature and pH not specified). Addition of penG failed to produce significant changes in the exchange profile (on the minute time scale) and suggested a lack of large structural changes in BlaR^S upon acylation. Here, our amide hydrogen exchange measurements via NMR gave us access to shorter time scales (milliseconds) with greater spatial resolution. For most NHs, acylation caused insignificant differences in the exchange rate constants (k_{H_2O}). Thus, similar to the previous HX studies of *B. lichenformis* BlaR^S,[10] our k_{H_2O} rate constants suggest the overall structure of *S. aureus* BlaR^S is unchanged by acylation. We observed some local decreases in k_{H_2O}, particularly at the end of α-helix K. These differences, while small, suggest decreased solvent accessibility of β5/β6 hairpin amide protons and that acylation leads to some increased stability of NH hydrogen bonding.

More significant were the acylation-induced decreases in k_{NOE}, the cross-relaxation rates to Ser, Thr, and Tyr hydroxyl protons in rapid exchange with water. These decreases were prominent for residues in the antibiotic-binding pocket, suggesting that acylation expelled water from the binding pocket (Figure 5, right). A plausible explanation for this scenario is covalent binding of penG in the binding pocket. Inspection of the apo (PDB entry 1XA1) versus penG-acylated (PDB entry 1XA7) crystal structures[32] indicates that covalently bound penG would occupy ∼247 Å^3. In particular, the penG C6 substituent is comprised of a bulky hydrophobic phenyl group. Its insertion could expel water molecules, thereby reducing access of the Ser, Thr, and Tyr hydroxyl groups to water, resulting in the observed decreases in k_{NOE}. The notion of water expulsion upon acylation is consistent with the recent study by Kumarasiri and colleagues,[33] which showed the loss of a water molecule at the antibiotic-binding site in acylated versus apo BlaR^S.

A Model for Signal Transduction in BlaR^S. Our previous PRE studies[11] gave strong evidence of specific interaction between the β5/β6 hairpin of BlaR^S and the C-terminal residues of transmembrane loop 2 (L2). The interacting L2 residues formed an amphipathic helix, with hydrophobic residues facing away from the β5/β6−L2 interface to allow partial membrane embedding.

We now show that acylation by penG perturbs the conformational properties of this same β5/β6 region. Specifically, the β5/β6 region is intrinsically flexible. Acylation by penG causes CSPs in the β5/β6 residues, as well as changes in backbone dynamics on the subnanosecond and microsecond to millisecond time scales. The origins of these changes are suggested by the X-ray structure of penG-acylated BlaR^S (PDB entry 1XA7). The phenyl in the C6 substituent in penG is adjacent to β5/β6 residue I531, and comparisons of the two structures in the asymmetric unit suggest the side chain is mobile. Thus, both the CSPs and changes in local flexibility observed for the β5/β6 region by NMR could be explained in terms of dynamical interactions between the penG substituent (phenyl group) and mobile β5/β6 region.

We are therefore led to the following model for acylation and signal transduction (Figure 6). Acylation of BlaR^S by a β-lactam antibiotic would obviously impact the BlaR^S residues within the antibiotic-binding pocket, consistent with our NMR data. The pocket is intrinsically flexible (Figure 3) and can accommodate the acylated antibiotic with local rather than stark conformational rearrangements in the vicinity of the acylated Ser389. The bound antibiotic expels solvent, indicated by the reduced k_{NOE}, and reduces exchange broadening contributions to $J_{eff}(0)$ in the binding pocket: both consequences suggest a tightening of the protein "gut". Most critically, acylation introduces new dynamical interactions between the substituent of the bound antibiotic and residues bracketing the β5/β6 hairpin, in particular, I531. Those interactions rearrange or weaken the intrinsic contact between the β5/β6 hairpin and L2; the former scenario was indicated in our previous studies, but the latter could prevail *in vivo*. In either case, the perturbations of the β5/β6−L2 contact disturb the N-terminal end of transmembrane helix 3 and therefore the cytoplasmic protease domain. Thus, in our model, the antibiotic does not competitively disrupt the β5/β6−L2 contact. Rather, the BlaR^S antibiotic-binding pocket, the β5/β6 hairpin, L2, and transmembrane helix 3 form a chain of interaction that descends from the membrane surface to the cytoplasmic interior.

One would expect in this model that penicillin antibiotics with bulkier C6 substituents (C7 in cephalosporins) would inflict greater perturbations to the β5/β6−L2 contact, resulting in more effective signaling to the cytoplasm. In fact, recent studies by Llarrull et al. suggest that this is the case. The rank ordering of PC1 β-lactamase induction correlates with increasing the activity of the C6 substituent of penicillins, from least active to most active: penicillin G/ampicillin, then oxacillin/methicillin, and, finally, penicillin CBAP.[3]

Sequence-Specific Backbone Flexibility and Function. Conserved sequences reflect natural selection not only for specific chemical moieties and structure but also for functional motions.[34] In our model of Figure 6, I531 plays an important function by mediating contact between the antibiotic and β5/β6. One might therefore expect that I531 should be conserved across BlaR^S homologues. While I531 is not strictly conserved among the BlaR^S homologues, as analyzed by Wilke et al.,[8] it is functionally conserved, in that one sees either an isoleucine or valine at this position, thus indicating that an extended and branched hydrophobic side chain is likely important for function.[8] An exception is the class D β-lactamase OXA-10, a close structural homologue of BlaR^S (PDB entry 1FOF) with a 28% identical sequence. OXA-10 has the minimalist glycine at this position. This exception is intriguing from a functional standpoint, given that OXA-10 is an antibiotic resistance enzyme, rather than a membrane-associated sensor domain, as is the case for BlaR^S. In making this observation, we are not suggesting that a single-amino acid substitution would interconvert the sensor and enzyme functions. Rather, the OXA-10 exception likely highlights a local region of inter-residue interactions critical for function. Moreover, it illustrates how protein sequences can reflect the natural selection of function, an observation also documented by Kumarasiri et al.

DOI: 10.1021/bi501463k
Biochemistry 2015, 54, 1600−1610

for a different site for the same two proteins.[33] These two related proteins, one a sensor ($BlaR^S$) and the other an enzyme (OXA-10), illustrate how distinct evolutionary tangents can diversify function from a shared genetic blueprint.

Cryptic Allostery in $BlaR^S$. Beyond the antibiotic-binding site and $\beta5/\beta6$ hairpin, another region that shows persistent acylation-induced CSPs, altered $J_{eff}(0)$ values, and altered HX properties is α-helix K (Figure 2 and Figure 6C,D, yellow helix). These residues (e.g., A568, E569, L570, and G580) lack contact with the bound antibiotic and other BlaR1 domains. Thus, at first glance, their changes were hard to rationalize.

However, recent computational studies by Bowman and Geissler[30] raise an interesting possibility. These investigators developed Markov-state models (MSM) for the TEM-1 β-lactamase, a structural homologue of $BlaR^S$. Their models revealed three transient pockets outside the antibiotic-binding site, available for ligand binding. These pockets are a direct consequence of TEM-1 intrinsic conformational dynamics and result from correlated side chain motions that leave the backbone conformation intact. The transient nature of these pockets makes their detection difficult by standard structural analyses. Accordingly, they have been called "cryptic allosteric sites",[30] and they represent potential sites of binding by ligands. One of the three TEM-1 cryptic sites is located in its $\beta5/\beta6$ hairpin that is homologous to that in $BlaR^S$. The other two cryptic sites coincide with residues that were previously established to bind an allosteric ligand [*N*,*N*-bis(4-chlorobenzyl)-1*H*-1,2,3,4-tetraazol-5-amine, or CBT].[35,36] These two sites are between TEM-1 α-helix K and the middle of the TEM-1 $\beta4/\beta5$ sheet. Remarkably, this TEM-1 region is homologous to the $BlaR^S$ helix K region highlighted by this study (Figure 6C,D, yellow helix).

Thus, the cryptic allosteric sites of the TEM-1 β-lactamase predicted by Markov-state models overlap with the sites of dynamic changes in $BlaR^S$ as revealed by NMR. This raises the interesting possibility that $BlaR^S$ might also harbor cryptic allosteric sites.

CONCLUDING REMARKS

We have investigated the conformational dynamics of $BlaR^S$ and its response to acylation by a β-lactam antibiotic, penG. Our results reveal insights into the mechanism for transmembrane signal transduction that entails a contiguous path from the $BlaR^S$ antibiotic-binding site to the cytoplasm via contact between the $\beta5/\beta6$ hairpin and extracellular loop L2. Acylation by β-lactam antibiotic results in dynamic interactions between the bound antibiotic and residues of the adjacent $\beta5/\beta6$ hairpin, which then perturb the $\beta5/\beta6$–L2 interaction, and thence to the transmembrane helices.

Elucidating the complete signal transduction mechanism requires further work and likely involves additional factors. Nevertheless, our investigations of conformational fluctuations in BlaR1 make a significant step forward. They show experimental evidence of a contiguous path of interactions allowing transmembrane signal transduction, thus providing the first insights into the process of the BlaR1 protein of MRSA, an important human pathogen.

ASSOCIATED CONTENT

Supporting Information

Seven figures (Figures S1–S7) showing exemplary 2D ^{15}N–^{1}H spectra, the status of backbone assignments, bar charts for $J_{eff}(0)$ and hydrogen exchange rate constants, LTS data, and mass spectrometry data and values of $J_{eff}(0)$ and hydrogen exchange parameters (Tables S1 and S2). This material is available free of charge via the Internet at http://pubs.acs.org.

AUTHOR INFORMATION

Corresponding Author

*E-mail: jpeng@nd.edu. Telephone: (574) 631-2983. Fax: (574) 631-6652.

Funding

This work was supported by National Institutes of Health (NIH) Grants GM085109 (to J.W.P.) and AI104987 (to S.M.) and NIH Training Grant T32GM075762 (to T.E.F.).

Notes

The authors declare no competing financial interest.

ACKNOWLEDGMENTS

We are grateful for discussions with Mr. Daniel Mulhall, Dr. Xingsheng Wang, Dr. Petra Rovo, Dr. Michelle Joyce, and Dr. Leticia Llarrull.

ABBREVIATIONS

2D, two-dimensional; PRE, paramagnetic relaxation enhancement; EXSY, exchange spectroscopy; HX, hydrogen exchange; HSQC, heteronuclear single-quantum correlation; rmsd, root-mean-square deviation.

REFERENCES

(1) Fisher, J. F., Meroueh, S. O., and Mobashery, S. (2005) Bacterial resistance to β-lactam antibiotics: Compelling opportunism, compelling opportunity. *Chem. Rev. 105*, 395–424.

(2) Llarrull, L. I., Fisher, J. F., and Mobashery, S. (2009) Molecular basis and phenotype of methicillin resistance in *Staphylococcus aureus* and insights into new β-lactams that meet the challenge. *Antimicrob. Agents Chemother. 53*, 4051–4063.

(3) Llarrull, L. I., Toth, M., Champion, M. M., and Mobashery, S. (2011) Activation of BlaR1 protein of methicillin-resistant *Staphylococcus aureus*, its proteolytic processing, and recovery from induction of resistance. *J. Biol. Chem. 286*, 38148–38158.

(4) Cha, J., Vakulenko, S. B., and Mobashery, S. (2007) Characterization of the β-lactam antibiotic sensor domain of the MecR1 signal sensor/transducer protein from methicillin-resistant *Staphylococcus aureus*. *Biochemistry 46*, 7822–7831.

(5) Wilke, M. S., Lovering, A. L., and Strynadka, N. C. (2005) β-Lactam antibiotic resistance: A current structural perspective. *Curr. Opin. Microbiol. 8*, 525–533.

(6) Golemi-Kotra, D., Cha, J. Y., Meroueh, S. O., Vakulenko, S. B., and Mobashery, S. (2003) Resistance to β-lactam antibiotics and its mediation by the sensor domain of the transmembrane BlaR signaling pathway in *Staphylococcus aureus*. *J. Biol. Chem. 278*, 18419–18425.

(7) Thumanu, K., Cha, J., Fisher, J. F., Perrins, R., Mobashery, S., and Wharton, C. (2006) Discrete steps in sensing of β-lactam antibiotics by the BlaR1 protein of the methicillin-resistant *Staphylococcus aureus* bacterium. *Proc. Natl. Acad. Sci. U.S.A. 103*, 10630–10635.

(8) Wilke, M. S., Hills, T. L., Zhang, H. Z., Chambers, H. F., and Strynadka, N. C. (2004) Crystal structures of the Apo and penicillin-acylated forms of the BlaR1 β-lactam sensor of *Staphylococcus aureus*. *J. Biol. Chem. 279*, 47278–47287.

(9) Birck, C., Cha, J. Y., Cross, J., Schulze-Briese, C., Meroueh, S. O., Schlegel, H. B., Mobashery, S., and Samama, J. P. (2004) X-ray crystal structure of the acylated β-lactam sensor domain of BlaR1 from *Staphylococcus aureus* and the mechanism of receptor activation for signal transduction. *J. Am. Chem. Soc. 126*, 13945–13947.

(10) Hanique, S., Colombo, M. L., Goormaghtigh, E., Soumillion, P., Frere, J. M., and Joris, B. (2004) Evidence of an intramolecular

DOI: 10.1021/bi501463k
Biochemistry 2015, 54, 1600–1610

interaction between the two domains of the BlaR1 penicillin receptor during the signal transduction. *J. Biol. Chem. 279*, 14264−14272.
(11) Frederick, T. E., Wilson, B. D., Cha, J., Mobashery, S., and Peng, J. W. (2014) Revealing cell-surface intramolecular interactions in the BlaR1 protein of methicillin-resistant *Staphylococcus aureus* by NMR spectroscopy. *Biochemistry 53*, 10−12.
(12) Cavanagh, J., Fairbrother, W., Palmer, A., III, Skelton, N., and Rance, M. (2006) *Protein NMR Spectroscopy: Principles and Practice*, 2nd ed., pp 613−656, Academic Press, New York.
(13) Goddard, T., and Kneller, D. (2009) *Sparky 3*, University of California, San Francisco.
(14) Keller, R. (2004) Optimizing the process of nuclear magnetic resonance spectrum analysis and computer aided resonance assignment. ETH, Zurich.
(15) Pervushin, K., Riek, R., Wider, G., and Wuthrich, K. (1997) Attenuated T2 relaxation by mutual cancellation of dipole-dipole coupling and chemical shift anisotropy indicates an avenue to NMR structures of very large biological macromolecules in solution. *Proc. Natl. Acad. Sci. U.S.A. 94*, 12366−12371.
(16) Ferrage, F., Reichel, A., Battacharya, S., Cowburn, D., and Ghose, R. (2010) On the measurement of ^{15}N-{^{1}H} nuclear Overhauser effects. 2. Effects of the saturation scheme and water signal suppression. *J. Magn. Reson. 207*, 294−303.
(17) Farrow, N. A., Zhang, O., Szabo, A., Torchia, D. A., and Kay, L. E. (1995) Spectral density function mapping using ^{15}N relaxation data exclusively. *J. Biomol. NMR 6*, 153−162.
(18) Ishima, R., and Nagayama, K. (1995) Protein backbone dynamics revealed by quasi spectral density function analysis of amide N-15 nuclei. *Biochemistry 34*, 3162−3171.
(19) Peng, J. W., and Wagner, G. (1995) Frequency spectrum of NH bonds in eglin c from spectral density mapping at multiple fields. *Biochemistry 34*, 16733−16752.
(20) Lipari, G., and Szabo, A. (1982) Model-Free Approach to the Interpretation of Nuclear Magnetic Resonance Relaxation in Macromolecules. 1. Theory and Range of Validity. *J. Am. Chem. Soc. 104*, 4546−4559.
(21) Lipari, G., and Szabo, A. (1982) Model-free Approach to the Interpretation of Nuclear Magnetic Resonance Relaxation of Macromolecules. 2. Analysis of Experimental Results. *J. Am. Chem. Soc. 104*, 4559−4570.
(22) Fitzkee, N. C., Torchia, D. A., and Bax, A. (2011) Measuring rapid hydrogen exchange in the homodimeric 36 kDa HIV-1 integrase catalytic core domain. *Protein Sci. 20*, 500−512.
(23) Kupce, E., Boyd, J., and Campbell, I. D. (1995) Short selective pulses for biochemical applications. *J. Magn. Reson., Ser. B 106*, 300−303.
(24) Englander, S. W., and Kallenbach, N. R. (1983) Hydrogen exchange and structural dynamics of proteins and nucleic acids. *Q. Rev. Biophys. 16*, 521−655.
(25) Li, F., Schafer, R., Hwang, C. T., Tanner, C. E., and Ruggiero, S. T. (2010) High-precision sizing of nanoparticles by laser transmission spectroscopy. *Appl. Opt. 49*, 6602−6611.
(26) Li, F., Mahon, A. R., Barnes, M. A., Feder, J., Lodge, D. M., Hwang, C. T., Schafer, R., Ruggiero, S. T., and Tanner, C. E. (2011) Quantitative and rapid DNA detection by laser transmission spectroscopy. *PLoS One 6*, e29224.
(27) Goffin, C., and Ghuysen, J. M. (2002) Biochemistry and comparative genomics of SxxK superfamily acyltransferases offer a clue to the mycobacterial paradox: Presence of penicillin-susceptible target proteins versus lack of efficiency of penicillin as therapeutic agent. *Microbiol. Mol. Biol. Rev. 66*, 702−738.
(28) Chen, K., and Tjandra, N. (2011) Water proton spin saturation affects measured protein backbone ^{15}N spin relaxation rates. *J. Magn. Reson. 213*, 151−157.
(29) Lakomek, N. A., Ying, J., and Bax, A. (2012) Measurement of ^{15}N relaxation rates in perdeuterated proteins by TROSY-based methods. *J. Biomol. NMR 53*, 209−221.
(30) Bowman, G. R., and Geissler, P. L. (2012) Equilibrium fluctuations of a single folded protein reveal a multitude of potential cryptic allosteric sites. *Proc. Natl. Acad. Sci. U.S.A. 109*, 11681−11686.
(31) Fersht, A. (1985) *Enzyme Structure and Mechanism*, 2nd ed., W. H. Freeman and Co., New York.
(32) *maestro*, version 9.3.5 (2012) Schrödinger, LLC, New York.
(33) Kumarasiri, M., Llarrull, L. I., Borbulevych, O., Fishovitz, J., Lastochkin, E., Baker, B. M., and Mobashery, S. (2012) An amino acid position at crossroads of evolution of protein function: Antibiotic sensor domain of BlaR1 protein from *Staphylococcus aureus* versus clasS D β-lactamases. *J. Biol. Chem. 287*, 8232−8241.
(34) Peng, T., Zintsmaster, J. S., Namanja, A. T., and Peng, J. W. (2007) Sequence-specific dynamics modulate recognition specificity in WW domains. *Nat. Struct. Mol. Biol. 14*, 325−331.
(35) Wang, X., Minasov, G., and Shoichet, B. K. (2002) Evolution of an antibiotic resistance enzyme constrained by stability and activity trade-offs. *J. Mol. Biol. 320*, 85−95.
(36) Horn, J. R., and Shoichet, B. K. (2004) Allosteric inhibition through core disruption. *J. Mol. Biol. 336*, 1283−1291.
(37) Llarrull, L. I., and Mobashery, S. (2012) Dissection of events in the resistance to β-lactam antibiotics mediated by the protein BlaR1 from *Staphylococcus aureus*. *Biochemistry 51*, 4642−4649.

DOI: 10.1021/bi501463k
Biochemistry 2015, 54, 1600−1610